BIO-06-1183

Modeling Transition to Turbulence in Eccentric Stenotic Flows

Sonu S. Varghese and Steven H. Frankel

School of Mechanical Engineering,

Purdue University, 585 Purdue Mall,

West Lafayette, IN 47907, USA

Paul F. Fischer

Argonne National Laboratories, Argonne, IL 60439, USA

(Dated: March 28, 2007)

Abstract

Mean flow predictions obtained from a host of turbulence models were found to be in poor agreement with recent direct numerical simulation results for turbulent flow distal to an idealized eccentric stenosis. Many of the widely used turbulence models, including a large eddy simulation model, were unable to accurately capture the post-stenotic transition to turbulence. The results suggest that efforts towards developing more accurate turbulence models for low Reynolds number, separated transitional flows are necessary before such models can be used confidently under hemodynamic conditions where turbulence may develop.

I. INTRODUCTION

Experimental and numerical evidence for irregular, transitional, and turbulent hemodynamic flows in both physiological (due to vessel curvature and bifurcations) and pathological (due to plaque-induced stenoses) situations is widely available[1–3]. The ability of such flows to produce hemodynamic forces (through pressure and vessel shear stress) and mass transport conditions conducive to disease progression, such as in the case of atherosclerosis, is also appreciated[4–6]. Due to obvious limitations related to making *in vivo* measurements of flow and flow forces in stenosed arterial vessels, computational fluid dynamics (CFD) has begun to play a major role in studyiung hemodynamic, arterial, and stenotic flows over the past decade or so. CFD stenotic flow studies have considered both steady and pulsatile stenotic flows, coupled with fluid-structure interactions, non-Newtonian effects, and realistic geometries reconstructed from clinical MRI data[7–10]. One of the main obstacles to overcome in applying CFD to study pathological hemodynamics, such as in stenotic flows, is related to accurate numerical simulations and/or modeling irregular flows accounting for the possibility of transitional and turbulent flow.

Notable studies that have addressed the issue of post-stenotic transition to turbulence include the high-order simulations by Mallinger and Drikakis [11] and the large eddy simulations (LES) by Mittal *et al.* [12], both of which imposed small, white-noise, random perturbations on the inflow velocity to break the flow symmetry. Sherwin and Blackburn[13] conducted stability analyses of steady and pulsatile, axisymmetric stenotic flows using stenosis models similar to those employed by Ahmed and Giddens[14–16] in their classical experiments. Their study showed that inlet flow disturbances (or upstream noise) can trigger transition in the post-stenotic region. Most recently, Varghese, Frankel and Fischer[17,18] employed direct numerical simulations (DNS) to provide a detailed representation and analysis of the flow field distal to clinically significant, albeit idealized, stenoses models under physiologically realistic flow conditions. Both steady and pulsatile flow were simulated through these smoothly contoured stenosed vessels (maximum area reduction of 75%) with the flow model and parameters selected to match the stenotic flow experiments of Ahmed and Giddens[14,16] and in the absence of any inflow disturbances, DNS predicted a laminar flow field downstream of an axisymmetric stenosis. However, their study illustrated that even a small stenosis asymmetry, in the form of an eccentricity that was only 5% of the main vessel diameter, can

trigger post-stenotic transition to turbulence. Transition to turbulence manifested itself in large temporal and spatial gradients of wall shear stress (WSS), with the turbulent region witnessing a sharp amplification in instantaneous magnitudes.

While DNS is clearly a very useful tool for accurately simulating stenotic flows, the ability to predict such flows at a reduced computational cost, perhaps with a suitably developed turbulence model, would be useful in studying flows through realistic arterial geometries. There is a great variety of turbulence models available through commercial CFD vendors today, especially two-equation models, that employ the Reynolds averaged Navier Stokes (RANS) approach to predict the mean flow. However it is important to understand the limitations of these models, most of which have been developed using knowledge of simple classes of well-behaved two-dimensional flows[19]. This begs the question whether it is even appropriate to consider the use of turbulence models to capture, or model the effects of, disparate features of a post-stenotic flowfield such as separation, recirculation, strong shear layers, localized transition to turbulence and relaminarization. In short, a complete three-dimensional flowfield[17,18].

The first-order level of RANS modeling, incorporated in the popular two-equation variants, involves the eddy viscosity model that is based on the Boussinesq assumption. This approach, which basically assumes isotropic turbulence and fails to account for transport of turbulent stresses, would seem especially problematic given the anistropic nature of stenotic jet breakdown demonstrated by DNS. The second-order turbulence models form the logical level within the RANS framework, with separate equations solved for each component of the turbulent (Reynolds) stress, towards the goal of capturing stress anisotropy and accounting for effects such as high strain-rate changes, streamline curvature and rotation, all of which produce unequal turbulent stresses. The most advanced of these, the Reynolds stress model (RSM), requires significant computational resources to solve the additional transport equations and it is also limited by the fact that several terms in these equatons have to be modeled. As one may expect, the advantage of this model can be compromised if these terms are modeled inaccurately.

In earlier works using the unsteady RANS approach, Varghese and Frankel [20] and Ryval *et al.*[21] showed that the the two-equation low-Reynolds number $k-\omega$ model has potential to predict stenotic flows. Both studies employed the original axisymmetric stenosis model used by Ahmed and Giddens[14] in their experiments to allow for validation. However, as mentioned

earlier, under both steady and pulsatile inflow conditions, stability analysis and DNS have shown that inlet flow perturbations can cause transition to turbulence in the post-stenotic flowfield at the Reynolds numbers used in the experiments[13,17,18]. Given the uncertainty in quantifying the level of upstream disturbance, whether or not final conclusions regarding the abilities of turbulence models can be drawn from the RANS studies cited above[20,21] (including one by two of the current authors) is an open question. This is not to cast doubt on the the RANS results by themselves, only to question the efficacy of validation.

An important by-product of the DNS work of Varghese *et al.* is that an extensive dataset for a demonstrably turbulent post-stenotic flow field now exists, one which can be used to establish the reliability of available turbulence models. The advantage here is that the perturbation used to trigger transition for the DNS is a quantifiable entity, the stenosis eccentricity itself, as opposed to upstream disturbances (which were absent in the DNS). As the authors note, the geometric asymmetry is extremely relevant since real-life stenoses are unlikely to be perfectly axisymmetric and in addition, the Reynolds numbers at which the simulations were performed are physiologically relevant. As discussed above, the test is an extremely challenging one for RANS models and we focus on their abilities to model the flow under steady inflow conditions. The different turbulence models examined are all implemented in the commercially available computational fluid dynamics software FLUENT 6.2, arguably amongst the more popular of CFD codes within the biofluid modeling community. More details on the mathematical formulation and implementation of the models can be found in Wilcox's book on turbulence modeling[22] and the FLUENT manual[23].

II. STEADY FLOW THROUGH THE ECCENTRIC STENOSIS: RANS

A. Flow Model

Profiles of the eccentric stenosis model used by Varghese *et al*[17,18] are shown in figure 1 (the axisymmetric model is also shown for comparison). A cosine function dependent on the axial coordinate, x, was used to generate the axisymmetric geometry. The cross-stream

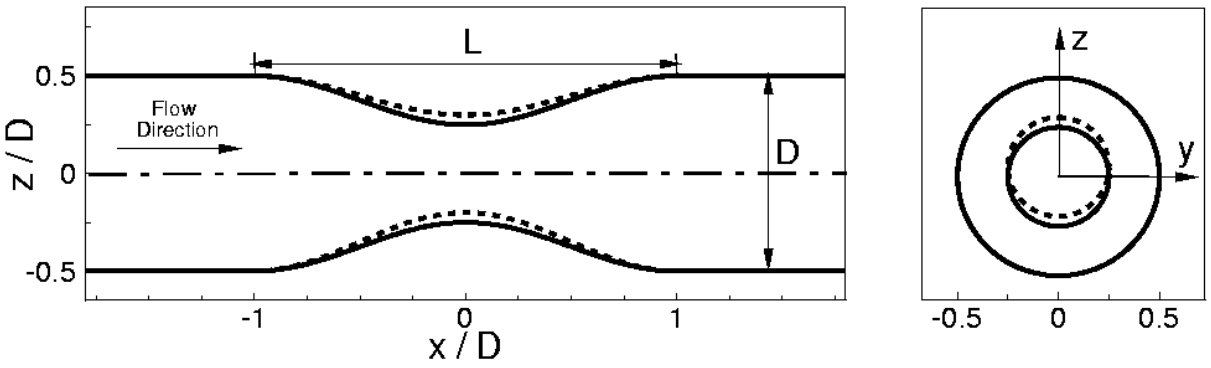

FIG. 1: Side and front views of the stenosis geometry ($L = 2D$), the solid line corresponding to the profile of the axisymmetric model and the dashed line to the eccentric model; x is the streamwise direction while y and z are the cross-stream directions. The front view shows the cross-section corresponding to both models in the main vessel and at the throat, $x = 0.0$.

coordinates, y and z, were computed by using $S(x)$, specifying the shape of the stenosis as

$$\begin{aligned} S(x) &= \tfrac{D}{2}[1 - s_o(1 + \cos\,(\tfrac{2\pi(\mathrm{x}-\mathrm{x_o})}{\mathrm{L}}))], \\ y &= S(x)\,\cos\,\theta, \\ z &= S(x)\,\sin\,\theta, \end{aligned} \tag{1}$$

where D is the diameter of the non-stenosed tube, $s_o = 0.25$ for the 75% area reduction stenosis used throughout this study, L is the length of the stenosis ($= 2D$ in this study), and x_o is the location of the center of the stenosis ($x_o - \frac{L}{2} \leq x \leq x_o + \frac{L}{2}$).

For the eccentric model, the stenosis axis was offset from the main vessel axis by $0.05D$. The offset, $E(x)$, and subsequently the modified y and z coordinates were computed as

$$\begin{aligned} E(x) &= \tfrac{s_o}{10}(1 + \cos\,(\tfrac{2\pi(\mathrm{x}-\mathrm{x_o})}{\mathrm{L}})), \\ y &= S(x)\,\cos\,\theta, \\ z &= E(x) + S(x)\,\sin\,\theta. \end{aligned} \tag{2}$$

Note that the offset was introduced in the $x - z$ plane ($y = 0.0$) only. The upstream and downstream sections of the vessel extended for three and twenty vessel diameters, respectively, as measured from the stenosis throat (located at $x = 0$ in the figure).

B. Problem Setup in FLUENT

The eccentric stenosis model described above was modeled and discretized using GAMBIT, the preprocessor for FLUENT, which is a finite volume based flow solver. The parabolic velocity profile for laminar, fully developed Poiseuille flow was specified at the inlet, placed three diameters upstream of the stenosis, exactly as in the DNS. The inlet velocity, fluid density and viscosity were set such that the Reynolds number based on main vessel diameter and mean inlet velocity was 1000. All results are normalized by the main vessel diameter (D) and the cross-sectional averaged inlet velocity (u_{in}). Turbulence intensity at the inlet boundary was set to zero, simulating a disturbance free inlet while gradient free boundary conditions were specified for all quantities at the outlet boundary, eighteen diameters downstream of the stenosis throat. Grid independence was established for all the cases reported here. For low Reynolds number flows, the turbulence models typically require the enhanced wall treatment option in FLUENT, so that the near-wall mesh is capable of resolving the viscous sublayer, with the first grid point off the wall lying in the region $y^+ \approx 1$. This was confirmed to be the case for all the calculations performed in this study.

The convective terms in the momentum and turbulence equations were discretized using second-order upwinding and pressure-velocity coupling was achieved using the SIMPLEC solver. All computations were coverged to residuals less than 10^{-5}. More details on the solver, turbulent flow parameters and modeling guidelines can be found in the FLUENT manual[23].

C. The Low-Reynolds Number $k-\omega$ Model

The two-equation low-Reynolds number $k-\omega$ model involves computing the eddy viscosity by solving transport equations for k and ω, representing physical processes that occur within the transitional or turbulent flowfield. Wilcox[22] has shown that this model has potential to predict transitional flows quite well and previous studies of stenotic flows have pointed to the low Reynolds number $k-\omega$ model as most suited to modeling such flows[20,21].

Figure 2(a) compares streamwise velocity profiles predicted by the low-Reynolds number $k-\omega$ model with DNS results. DNS tells us that the stenotic jet extends until $x \approx 11D$ before turbulent breakdown creates a more uniform velocity distribution across the vessel

cross-section. The model differs considerably by predicting that the jet extends only till $x \approx 5D$ before the velocity profiles start to take on a more uniform shape. As a result, the flow completely reattaches by this station whereas the simulations indicate that flow separation continues at least till $x = 10D$. This apparent early transition is confirmed by turbulent kinetic energy profiles in figure 3(a), with maximum k values occuring between $x = 2D$ and $3D$. In contrast, the DNS profiles (also shown in the same figure) predict maximum turbulent energy much further downstream from the stenosis throat, between $x = 8D$ and $10D$. At these locations, the model predicts negligible turbulent energy.

D. The Low Reynolds Number RNG and Realizable $k - \epsilon$ Models

The RNG $k-\epsilon$ model is a modification of the widely used standard $k-\epsilon$ epsilon in which the eddy viscosity is computed based on renormalization group theory[24–26]. The realizable $k - \epsilon$ model (RLZ) is a more recent addition to the class of two-equation models and was developed to satisfy certain mathematical constraints on the normal stresses, consistent with the physics of turbulent flows. The main advantage of the realizable model over its standard counterpart is its superior performance for highly strained flows involving strong adverse pressure gradients, separation and recirculation. While both the RNG and realizable $k - \epsilon$ models have improved prediction capabilities for flows featuring strong streamline curvature, vortices and rotation, it is not clear which of these performs better [23]. Both variants have improvements that would be deemed favorable with respect to the current problem.

Velocity profiles predicted by the RNG and realizable models, in figures 2(b) and 2(c), respectively, suggest that these models do not provide an improvement over the low Reynolds number $k - \omega$ model. Perhaps slightly worse. The profiles for the two models are fairly identical, with the stenotic jet extending only till $x \approx 3D$ and the flow completely reattaching by this location. Figures 3(b) and 3(c) show that the two $k - \epsilon$ variants predict maximum turbulent energy almost immediately downstream of the stenosis, between $x = 1D$ and $2D$, about one vessel diameter earlier than the $k - \omega$ model. As a result, we see the velocity profiles acquiring a more uniform nature as early as $x = 4D$.

The Boussinesq hypothesis governing the relation between the turbulent stresses and eddy viscosity in two-equation models results in the ratio between turbulent energy production and dissipation being significantly large in regions where the mean strain rate is high[27]. This

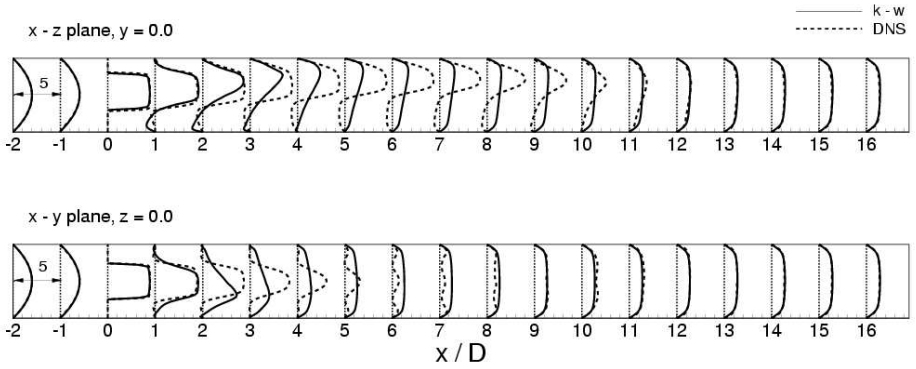

(a)

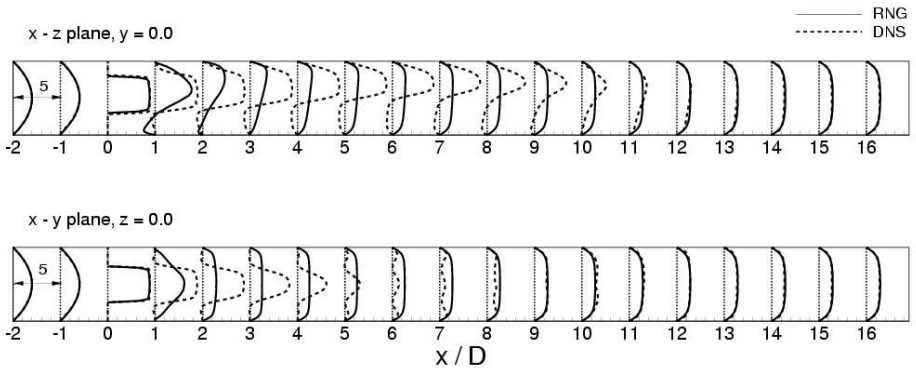

(b)

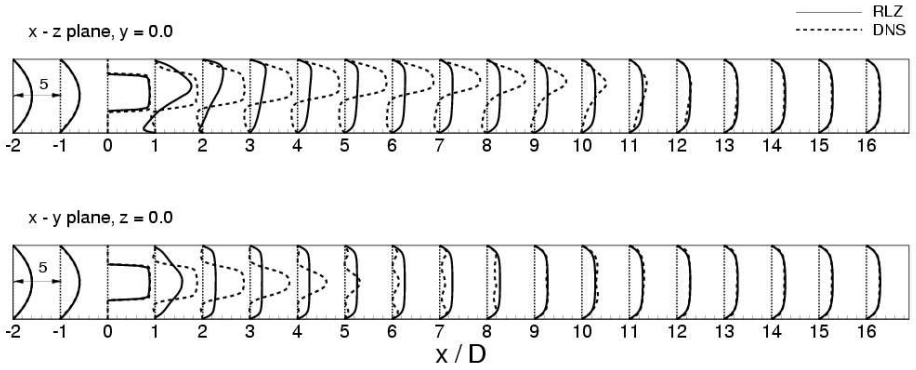

(c)

FIG. 2: Normalized streamwise velocity profiles, u/u_{in}, predicted by the two-equation turbulence models for steady flow through the eccentric stenosis. Corresponding DNS results are also shown. (a) Low Reynolds number $k-\omega$ model, (b) low Reynolds number RNG $k-\epsilon$ model, and (c) realizable $k-\epsilon$ model.

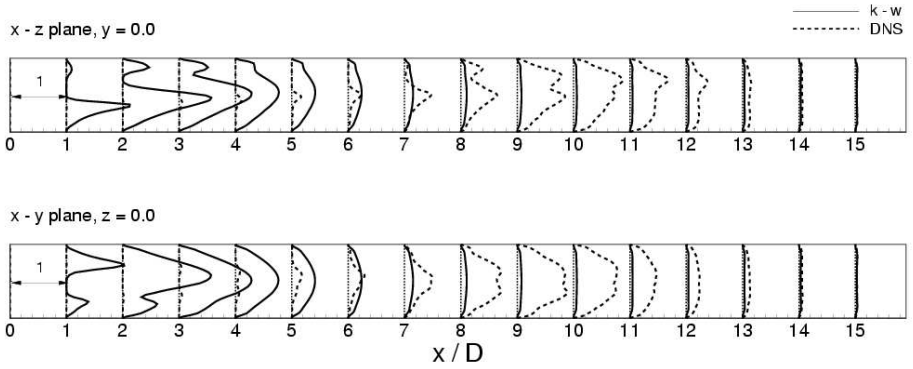

(a)

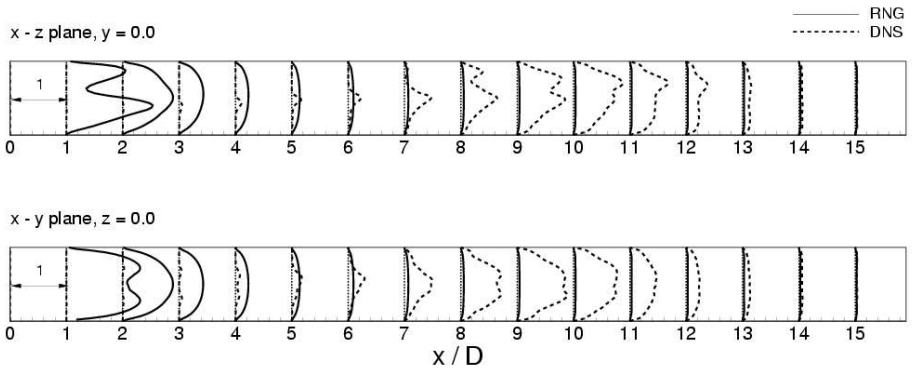

(b)

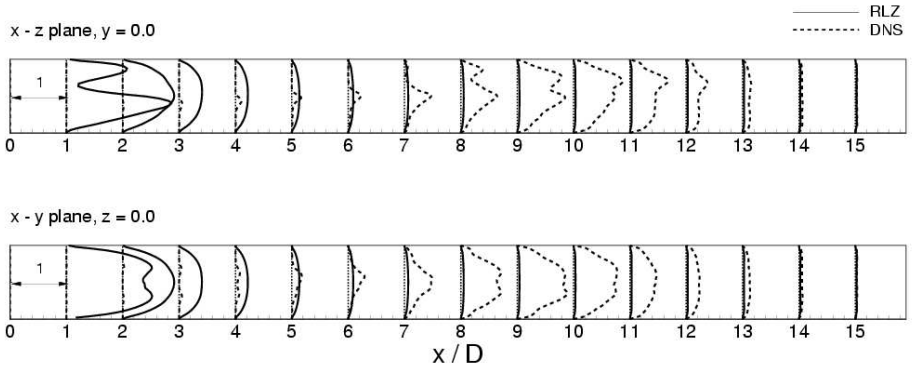

(c)

FIG. 3: Normalized turbulent kinetic energy profiles, k/u_{in}^2, predicted by the two-equation turbulence models for steady flow through the eccentric stenosis. Corresponding DNS results are also shown. (a) Low Reynolds number $k-\omega$ model, (b) low Reynolds number RNG $k-\epsilon$ model, and (c) realizable $k-\epsilon$ model.

results in abnormally large turbulent energy and stresses in the immediate post-stenotic shear layer, as the flow rapidly distorts, and perhaps explains why transition to turbulence is predicted several diameters upstream of where it occurred in the DNS.

E. The Shear Stress Transport (SST) $k-\omega$ Model

The two-equation models studied earlier do not account for the transport of turbulent shear stress, unlike Reynolds stress models. Menter[27] redefined the turbulent viscosity to account for this effect, deeming it necessary to improve predictions in adverse pressure gradient flows where flow separation occurs. The $k-\epsilon$ and $k-\omega$ are blended in such a way that the former is activated away from the wall and reduces to the latter close to the wall. The resulting shear stress transport (SST) model, led to significant improvements in the prediction of flows involving adverse pressure gradients (such as the backward facing step), especially due to its ability to account for transport of turbulent shear stress.

The characteristics of the current three-dimensional test case, its wall-boundedness and the origin of transition within the shear layer formed by the stenotic jet, suggest that the SST model would perhaps be more suited to predicting the flowfield more accurately than its traditional two-equation counterparts. Figure 4 compares time-averaged vorticity magnitude contours obtained with the DNS to contours predicted by the SST model, highlighting the poor performance of the model. The post-stenotic flowfield predicted by the SST model was not significantly different from that obtained using the standard low Reynolds number $k-\omega$ model. A probable cause of this lies in the formulation of the blending functions, which depend on the distance to the nearest wall [23], and in the current case, activates the $k-\omega$ throughout the flowfield. This is not surprising considering that the SST model, as used here, has been tested and calibrated for two-dimensional flows[27]. The blending functions in particular may have to be reformulated so as to predict complex, three-dimensional flows such as the stenotic flow problem, an exercise beyond the scope of this study.

F. The Reynolds Stress Model

As mentioned in the introduction, RSM offers several advantages over eddy viscosity models and in light of these, the results are rather dissapointing. In fact, axial velocity

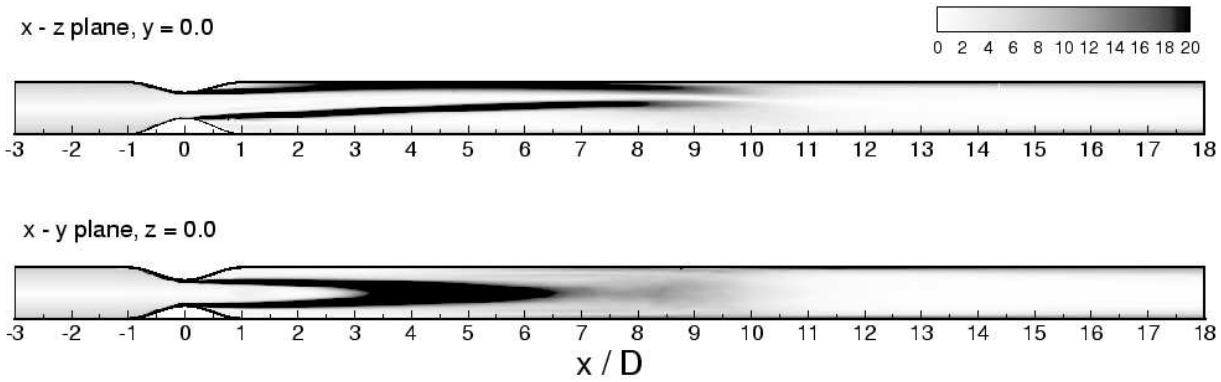

(a)

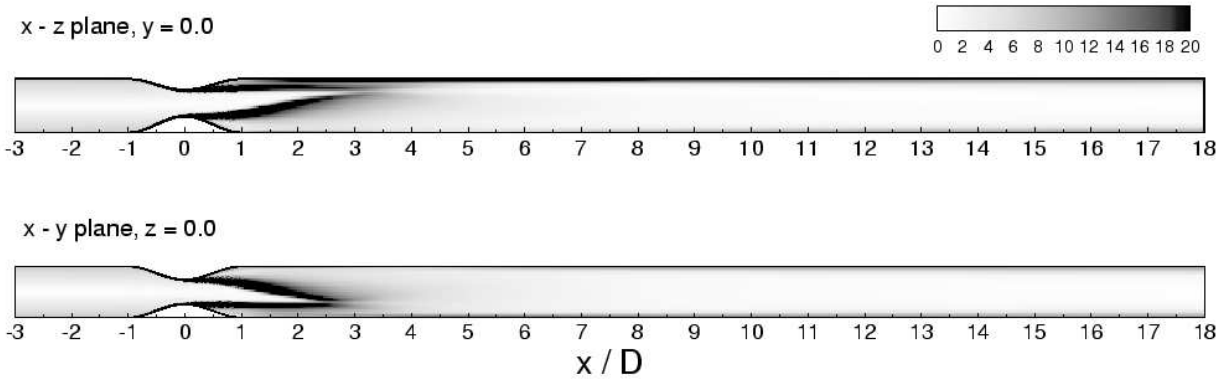

(b)

FIG. 4: Time-averaged vorticity magnitude contours for steady flow through the eccentric stenosis model at $Re = 1000$. (a) DNS, and (b) SST model. Levels have been normalized by u_{in}/D.

and turbulent kinetic energy results in figures 5(a) and 5(b), respectively, do not even show a significant improvement over the two-equation $k - \epsilon$ model variants. Complete flow reattachment occurs as early as three diameters downstream of the stenosis, while maximum values of turbulent kinetic energy are predicted immediately downstream of the stenosis, between $x = 1D$ and $x = 2D$. A possible explanation for this perhaps lies in the fact that the characteristic turbulence time and length scales used for modeling the terms in the stress transport equations are determined along the lines of the standard $k - \epsilon$ model.

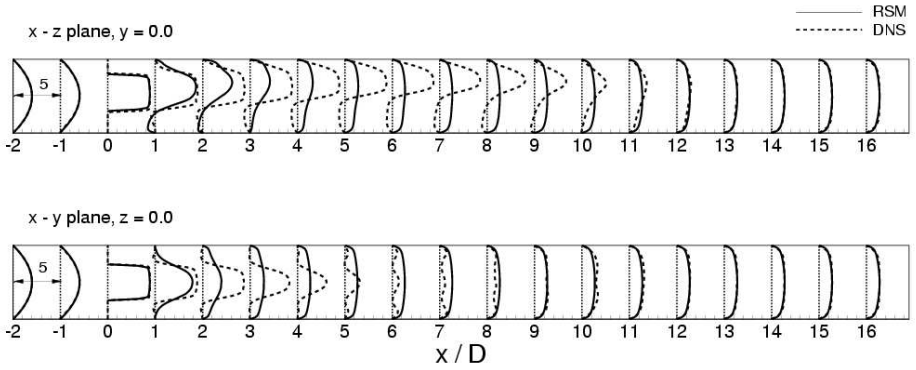

(a)

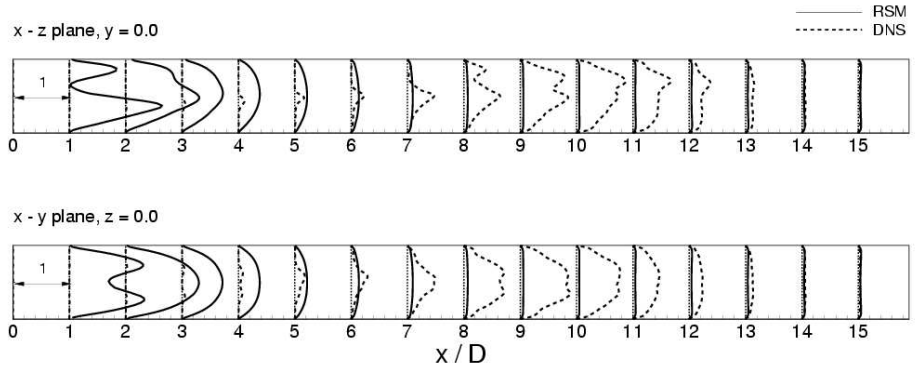

(b)

FIG. 5: Comparison of the Reynolds stress model (RSM) with DNS for steady flow through the eccentric stenosis. (a) Streamwise velocity profiles, normalized by mean inlet velocity, and (b) turbulent kinetic energy profiles, normalized by squared mean inlet velocity.

III. LARGE EDDY SIMULATIONS

The results in the previous sections demonstrate the inability of current turbulence models to adequately model transitional stenotic flows. Here we conduct preliminary investigations into the ability of LES, which lies in between the DNS and RANS modeling paradigm, to tackle stenotic flows. To date, only Mittal *et al* [12] have performed LES of the stenotic flow problem, though not from the standpoint of validation and simulation capability. For the sake of brevity, we avoid discussing the mathematical formulation of LES models, details of which can be found in the literature[22,28,29].

The problem setup for the eccentric stenosis model under steady inflow conditions was exactly similar to that for the turbulence model computations, since we were once again trying to replicate the DNS. Fully developed Poiseuille flow, free of disturbances, was specified at the inlet such that the Reynolds number based on main vessel diameter and mean inlet velocity was 1000 while gradient free boundary conditions were applied at the outlet. LES computations were performed on a grid comprising of approximately $700,000$ hexahedral cells, a mesh with more than double the number of cells for which grid independence was established for the RANS computations.

Bounded second-order central-differencing was employed to discretize the momentum equations and the PISO (pressure implicit with splitting of operators) algorithm was used for pressure-velocity coupling, the latter being recommended for transient flow calculations. Even though only the large scales are resolved in an LES, the range of scales is still significant and have to be resolved adequately. Upwinding schemes, used for the RANS calculations, are overly dissipative and consequently less accurate than central-differencing methods, which have low numerical diffusion properties[23,29]. LES is inherently unsteady since it solves for the instantaneous flow field, and second-order implicit time-stepping with a non-dimensional time-step size of $1.25e-3$ was used for temporal advancement. More details on LES implementation in FLUENT can be found in the manual[23].

Figure 6 compares instantaneous vorticity magnitude contours obtained with the DNS to similar contours obtained with FLUENTs LES formulation. Results are positive in that the jet breakdown in figure 6(b) appears to be occuring much further downstream from the stenosis as compared to the turbulence models tested earlier. However, due to time constraints, averaged quantities could not be obtained for more quantitative comparisons.

IV. CONCLUSIONS

A number of popular two-equation turbulence models were examined for their potential to predict flow through an eccentric stenosis model, used by Varghese *et al.*[17,18] in their DNS, under steady inflow conditions. The results clearly illustrated their inadequacy to model this type of three-dimensional flow. Even the Reynolds stress model does not perform any better since the assumptions that go into modeling some of the terms in the stress transport equations are similar to those used in the two-equation models. The poor performance of

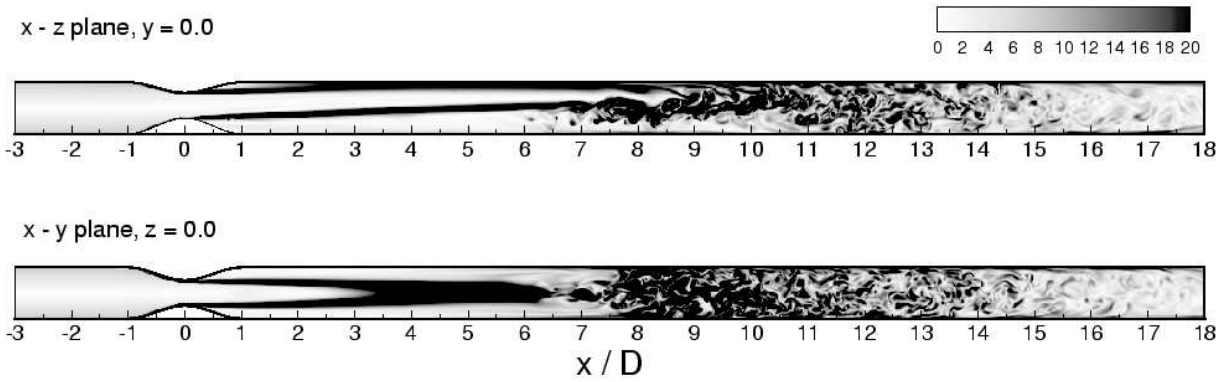

(a)

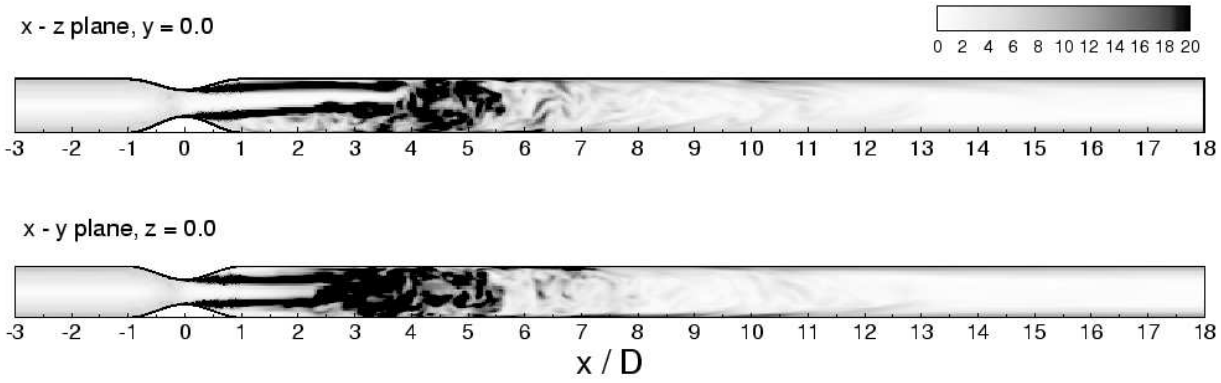

(b)

FIG. 6: Instantaneous vorticity magnitude contours for steady flow through the eccentric stenosis model at $Re = 1000$. (a) DNS (≈ 5.4 million grid points), and (b) Fluent LES ($\approx 700,00$ finite volume cells). Vorticity levels have been normalized by u_{in}/D.

these models under steady inflow conditions discouraged their validation under pulsatile inflow conditions. Preliminary LES work has indicated that this approach may offer a more promising route towards accurately predicting transitional stenotic flows, albeit at a greater computational cost than traditional turbulence models. Modeling along the lines of the SST model may offer potential benefits since it accounts for transport of turbulent stresses but extensive fine-tuning with DNS data may be required for satisfactory results.

Amongst the models not examined in this work is the detached eddy simulation (DES)

model, which belongs to a class of models that employ a RANS and LES coupling approach. The DES model in FLUENT is based on the one-equation Spallart-Allmaras model, involving the solution of a transport equation for a quantity that is similar to the turbulent eddy viscosity. It is typically employed for modeling high Reynolds number external aerodynamics [23] but given that the Boussinesq approach is employed for the Spallart-Allmaras model, the model may suffer from the same problems as the two-equation models studied here.

Acknowledgments

This work was supported in part by the Mathematical, Information, and Computational Sciences Division subprogram of the office of Advanced Scientific Computing Research, Office of Science, U.S. Department of Energy, under Contract DE-AC02-06CH11357.

---

[1] D. N. Ku. Blood flow in arteries. *Ann. Rev. Fluid Mech.*, 29:399–434, 1997.

[2] D. M. Wootton and D. N. Ku. Fluid mechanics of vascular systems, diseases, and thrombosis. *Annu. Rev. Biomed. Eng.*, 1:299–329, 1999.

[3] S.A. Berger and L-D. Jou. Flows in stenotic vessels. *Annual Rev. Fluid Mechanics*, 32:347–382, 2000.

[4] R. M. Nerem. Vascular fluid mechanics, the arterial wall, and atherosclerosis. *J. Biomech. Eng.*, 114:274–282, 1992.

[5] P. Libby. Inflammation in atherosclerosis. *Nature*, 420:868–874, 220.

[6] J. M. Tarbell. Mass transport in arteries and the localization of atherosclerosis. *Ann. Rev. Biomed. Eng.*, 5:79–118, 2003.

[7] D. Tang, J. Yang, C. Yang, and D.N. Ku. A nonlinear axisymmetric model with fluid-wall interactions for steady viscous flow in stenotic elastic tubes. *J. Biomech. Eng.*, 121:494–501, 1999.

[8] M. Bathe and R.D. Kamm. A fluid- structure interaction finite element analysis of pulsatile blood flow through a compliant stenotic artery. *J. Biomech. Eng.*, 121:361–369, 1999.

[9] J.R. Buchanan Jr., C. Kleinstreuer, and J.K. Comer. Rheological effects on pulsatile hemodynamics in a stenosed tube. *Comp. and Fluids*, 29:695–724, 2000.

[10] J.S. Stroud, S.A. Berger, and D. Saloner. Influence of stenosis morphology on flow through severely stenotic vessels: Implications for plaque rupture. *J. Biomech.*, 33:443–455, 2000.

[11] F. Mallinger and D. Drikakis. Instability in three-dimensional unsteady stenotic flows. *Int. J. Heat Fluid Flow*, 23:657–663, 2002.

[12] R. Mittal, S. P. Simmons, and F. Najjar. Numerical study of pulsatile flow in a constricted channel. *J. Fluid Mech.*, 485:337–378, 2003.

[13] S. J. Sherwin and H. M. Blackburn. Three-dimensional instabilities and transition of steady and pulsatile axisymmetric stenotic flows. *J. Fluid Mech.*, 533:297–327, 2005.

[14] S. A. Ahmed and D. P. Giddens. Velocity measurements in steady flow through axisymmetric stenoses at moderate Reynolds number. *J. Biomech.*, 16:505–516, 1983a.

[15] S. A. Ahmed and D. P. Giddens. Flow disturbance measurements through a constricted tube at moderate Reynolds numbers. *J. Biomech.*, 16:955–963, 1983b.

[16] S. A. Ahmed and D. P. Giddens. Pulsatile poststenotic flow studies with laser Doppler anemometry. *J. Biomech.*, 17:695–705, 1984.

[17] S. S. Varghese, S. H. Frankel, and P. F. Fischer. Direct numerical simulation of stenotic flows, Part 1: Steady flow. *Accepted for publication in Journal of Fluid Mechanics*, 2006.

[18] S. S. Varghese, S. H. Frankel, and P. F. Fischer. Direct numerical simulation of stenotic flows, Part 2: Pulsatile flow. *Accepted for publication in Journal of Fluid Mechanics*, 2006.

[19] K. Hanjalić. Advanced turbulence closure models: A view of current status and future prospects. *Int. J. Heat Fluid Flow*, 15:178–203, 1994.

[20] S. S. Varghese and S. H. Frankel. Numerical modeling of pulsatile turbulent flow in stenotic vessels. *J. Biomech. Eng.*, 125:445–460, 2003.

[21] J. Ryval, A. G. Straatman, and D. A. Steinman. Two-equation turbulence modeling of pulsatile flow in a stenosed tube. *J. Biomech. Eng.*, 126:625–635, 2004.

[22] D.C. Wilcox. *Turbulence Modeling for CFD.* DCW Industries, La Cañada, California, CA, 1993.

[23] *FLUENT Manual, Ver 6.2.*

[24] L.M. Smith and W.C. Reynolds. On the Yakhot-Orszag renormalization group method for deriving turbulence statistics and models. *Phys. Fluids A*, 4:364–390, 1992.

[25] V. Yakhot and S.A. Orszag. Renormalization group analysis of turbulence. *J. Scientific Computing*, 1:1–51, 1986.

[26] V. Yakhot and L.M. Smith. The renormalization group, the ϵ - expansion and derivation of turbulence models. *J. Scientific Computing*, 7:35–61, 1992.

[27] F. R. Menter. Two-equation eddy-viscosity turbulence models for engineering applications. *AIAA J.*, 32:1598–1605, 1994.

[28] M. Germano, U. Piomelli, P. Moin, and W. H. Cabot. A dynamic subgrid-scale eddy viscosity model. *Phys. Fluids A*, 3:1760–1765, 1991.

[29] U. Piomelli. Large-eddy simulation: achievements and challenges. *Prog. Aerospace Sci.*, 35:335–362, 1999.